We are IntechOpen, the world's leading publisher of Open Access books Built by scientists, for scientists

4,800
Open access books available

122,000
International authors and editors

135M
Downloads

Our authors are among the

154
Countries delivered to

TOP 1%
most cited scientists

12.2%
Contributors from top 500 universities

CLARIVATE ANALYTICS BOOK CITATION INDEX INDEXED

WEB OF SCIENCE™

Selection of our books indexed in the Book Citation Index in Web of Science™ Core Collection (BKCI)

Interested in publishing with us?
Contact book.department@intechopen.com

Numbers displayed above are based on latest data collected.
For more information visit www.intechopen.com

Real-time Obstacle Avoidance Using Potential Field for a Nonholonomic Vehicle

Hiroaki Seki, Yoshitsugu Kamiya and Masatoshi Hikizu
Kanazawa University
Japan

Fig. 1. Autonomous wheelchair moving through a narrow space.

1. Introduction

Obstacle avoidance is an important function for intelligent vehicles and mobile robots. Let's discuss about the obstacle avoidance for a nonholonomic vehicle (mobile robot) like an autonomous wheelchair (Fig. 1). It has two independently driven wheels and a body with a certain shape. If a vehicle can be treated as an omnidirectional movable point, numerous methods have been proposed and applied for it (Fig. 2). Collision free path can be easily found by artificial potential field (Khatib, 1986; Rimon & Koditsuchek, 1992), graph theory (Ulrich & Borenstein, 2000), sensor based method and so on. The problem for a nonholonomic vehicle with two independently driven wheels can come down to that for an omnidirectional point by approximating vehicle's shape to a circle with the center at the midpoint of two wheels. As shown in Fig. 3, obstacles should be expanded by the radius of the vehicle's circle and the

vehicle should be contracted to a point. However, it isn't reasonable to regard the rectangular body like a wheelchair as a circle and its circle sometimes can't pass through the narrow place where the original body can do.

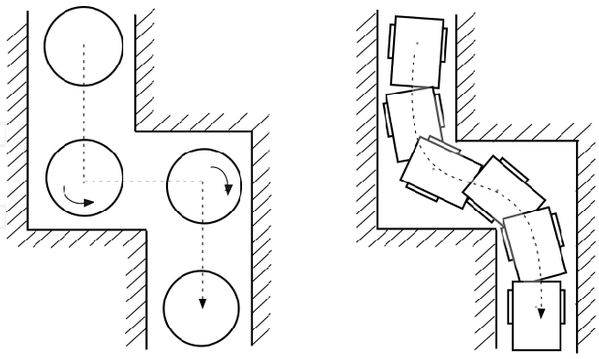

Fig. 2. Obstacle avoidance is easy for an omnidirectional vehicle, however, it is difficult for a vehicle with motion constraint and rectangular body.

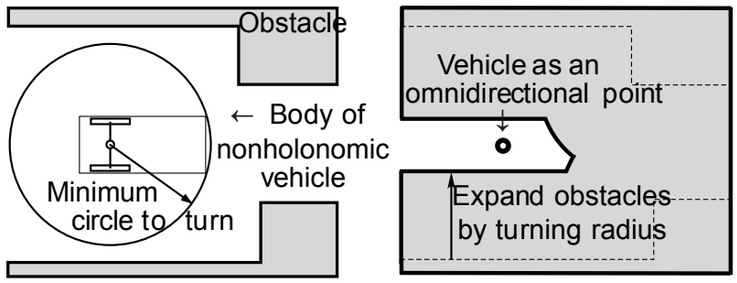

(a)Before expand obstacles (b) After expand obstacles

Fig. 3. Approximation of vehicle's shape by a circle for path planning.

In case of an omnidirectional (holonomic) vehicle, "configuration space" can be used for its path planning when the vehicle's shape is considered explicitly (Strobel, 1999). This problem is named "piano movers' problem" (Schwartz & Sharir, 2983). A set of position and orientation where a vehicle body doesn't collide with obstacles is represented by three dimensional configuration space (Fig. 4). A path of vehicle's position and orientation should be searched in this space by probabilistic roadmap method (Kavraki et al., 1996) for example. There are some studies considering both shape of vehicle's body and nonholonomic motion (Kondak & Hommel, 2001; Minguez et al., 2006; Ramirez & Zeghloul, 2001). It is very difficult problem to search a path in the configuration space under the motion constraint. Laumond (Laumond et al., 1994) solved this by modifying the collision free path obtained without motion constraint so as to satisfy motion constraint. Latombe (Latombe, 1991) proposed that the configuration space is divided into cells, the cells where a nonholonomic vehicle can move by simple motion such as turning, going straight, pulling over are connected by graph, and a path is searched in the graph. Anyway, these methods are too complicated for real-time obstacle avoidance using real sensor information although these ensure the solution of collision free path. Specially, calculation of configuration space needs much computing power.

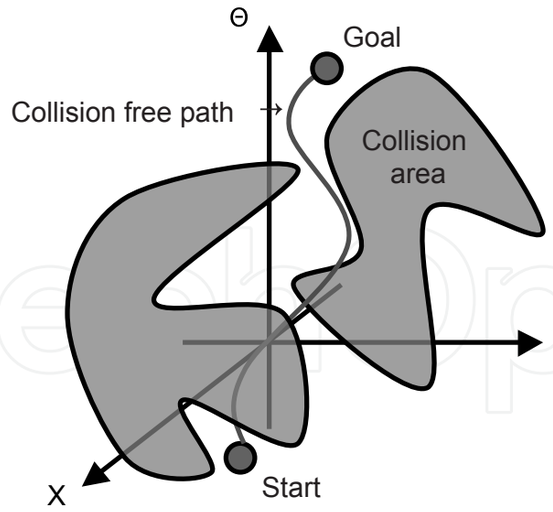

Fig. 4. 3D Configuration space for a vehicle with a certain shape

Therefore, we propose a practical method of local obstacle avoidance for a nonholonomic vehicle with rectangular body. Simple potential field using local sensor information of surrounding obstacles is applied.

2. Problem Statement

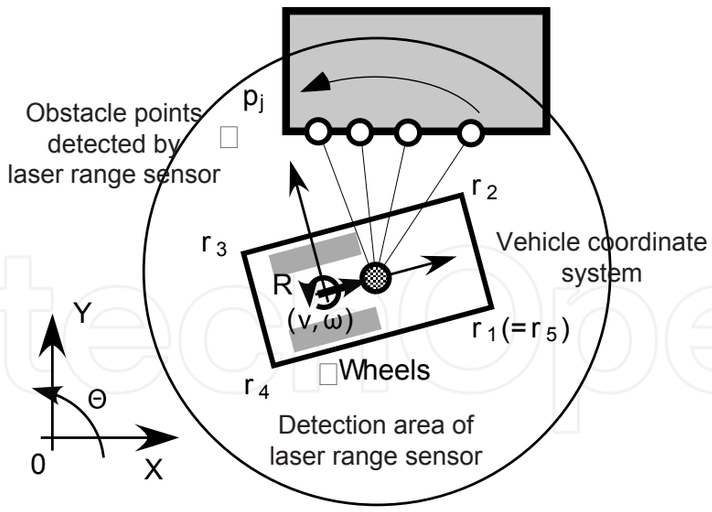

Fig. 5. Model of nonholonimic vehicle with a laser range sensor.

The obstacle avoidance problem to be solved is stated as follows.

1. We consider a nonholonomic vehicle with two independently driven wheels as shown in Fig. 5. It moves in a planar environment. The configuration of a vehicle is defined by $\boldsymbol{R} = (X, Y, \Theta)^T$ in the base coordinates, where (X, Y) is the position of the midpoint of

two wheels' axis and Θ is its orientation. The discrete kinematic model of this vehicle is written as

$$\begin{cases} X_n = X_{n-1} + v\Delta t \cos(\Theta_{n-1} + \frac{\omega \Delta t}{2}) \\ Y_n = Y_{n-1} + v\Delta t \sin(\Theta_{n-1} + \frac{\omega \Delta t}{2}) \\ \Theta_n = \Theta_{n-1} + \omega \Delta t \end{cases} \quad (1)$$

where Δt is the sampling time for control and $(v, \omega)^T$ are translational and rotational velocity. Suffix $n-1, n$ denote positions before and after the sampling time.

2. The shape of a vehicle is (or can be approximated by) a rectangle. Let the vertexes of the vehicle's shape be $\boldsymbol{r_i}(i = 1, 2, ..., n_r)$ in the vehicle coordinates.
3. A laser range sensor is mounted on the vehicle to detect obstacles. It has a circular detection area. Obstacles are scanned by this sensor every a certain angle. Let the detected points on the outline of obstacles be $\boldsymbol{p_j}(j = 1, 2, ..., n_p)$ in the vehicle coordinates. These points are called "obstacle points".
4. Global path planning is given. After the goal position of a vehicle $\boldsymbol{R_G} = (X_G, Y_G, \Theta_G)^T$ is given relatively near the start position, a local path to avoid obstacles is found. We explain the case that the start position is behind the goal position and a vehicle go forward to the goal. When a vehicle go backward to the goal, the front and back of the vehicle should be swapped.

3. Algorithm for Local Obstacle Avoidance

3.1 Outline

A method of local obstacle avoidance for a vehicle with two driven wheels and rectangular body is proposed. This outline is shown in Fig. 6. Basically, simple potential field is applied. Both an attractive force form the goal and repulsive forces from obstacles act on the vehicle and the resultant force moves the vehicle (Fig. 7). Main differences between the general method using potential field and our proposed method are following two points.

- In order to consider the motion constraint that a vehicle can't move just beside, two points of action where the attractive and repulsive forces act are placed on the front and rear body of a vehicle. Their forces at two points are treated as they work on a "lever" of which the fulcrum is the midpoint of two wheels.
- In order to consider the shape of vehicle's body, repulsive forces form obstacles are determined by the distances between obstacle points and the outline of vehicle's body.

This idea can simply introduce the consideration about the motion constraint and the vehicle's shape into the potential field method. Proposed method needs almost same computing power as general potential field method because their calculations have little difference. Since the data of a laser range sensor (obstacle points) can be used directly, this method is suitable for real-time obstacle avoidance. However, this also has a disadvantage of the local minima problem.

Then, our proposed method is explained in detail in the following sections. The generation of forces and the determination of vehicle's velocity are treated on the vehicle coordinate system.

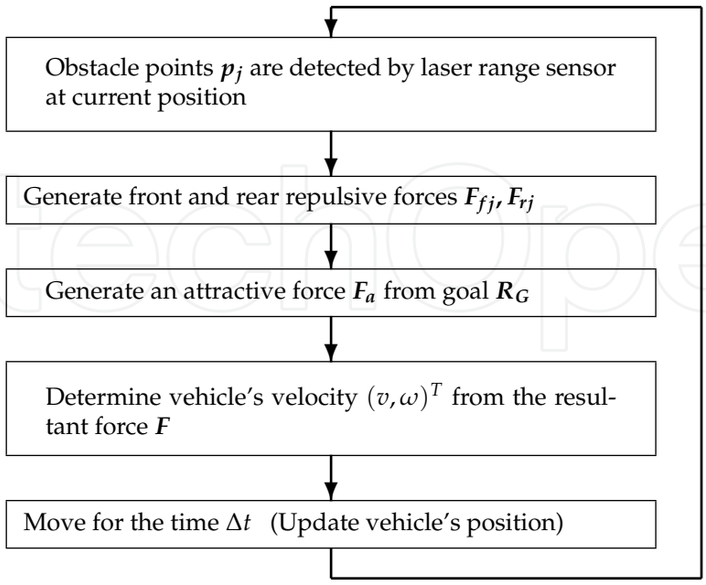

Fig. 6. Flowchart of proposed algorithm for obstacle avoidance.

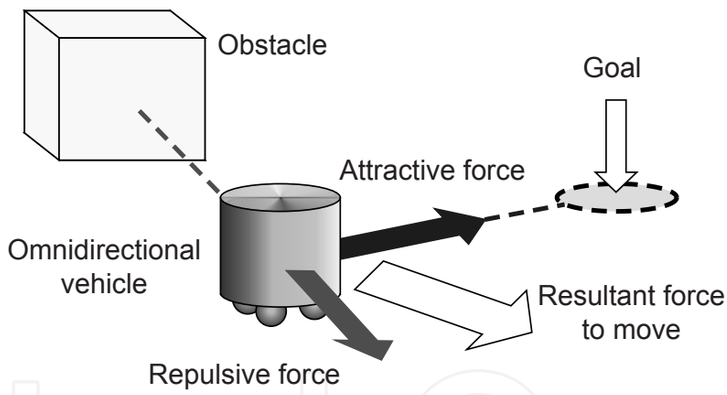

Fig. 7. Basic potential field method for omnidirectional vehicle to avoid obstacles

3.2 Generation of attractive and repulsive forces

Two action points of forces are placed at the front end and the rear end of a vehicle's body as shown in Fig. 8. Let the front end be $\boldsymbol{r_f} = (x_f, 0)^T$, and the rear end be $\boldsymbol{r_r} = (-x_r, 0)^T$ in the vehicle coordinate system. These points should not always be placed at the ends of a vehicle, however, acting forces at the ends makes vehicle's motion stable. When a obstacle point $\boldsymbol{p_j} = (p_{jx}, p_{jy})^T$ is detected in front of the line of two wheels' axes (y axis), a repulsive force $\boldsymbol{F_{fj}}$ is generated at the front point of action. When a obstacle point is behind this line, a repulsive force $\boldsymbol{F_{rj}}$ is generated at the rear point of action. The magnitudes of their forces are changed in inverse proportion to the squares of the distances between obstacle points and a

vehicle's body. Then, their forces are given by

$$\boldsymbol{F}_{fj} = \frac{K}{|\boldsymbol{q}_{fj} - \boldsymbol{p}_j|^2} \frac{\boldsymbol{r}_f - \boldsymbol{p}_j}{|\boldsymbol{r}_f - \boldsymbol{p}_j|}, \quad \text{if } p_{jx} > 0 \tag{2}$$

$$\boldsymbol{F}_{rj} = \frac{K}{|\boldsymbol{q}_{rj} - \boldsymbol{p}_j|^2} \frac{\boldsymbol{r}_r - \boldsymbol{p}_j}{|\boldsymbol{r}_r - \boldsymbol{p}_j|}, \quad \text{if } p_{jx} < 0 \tag{3}$$

where $\boldsymbol{q}_{fj}$, $\boldsymbol{q}_{rj}$ are the intersections of the vehicle's body and the segments between obstacle points and the action points $\boldsymbol{r}_f$, $\boldsymbol{r}_r$ respectively. K is the coefficient of repulsive force.

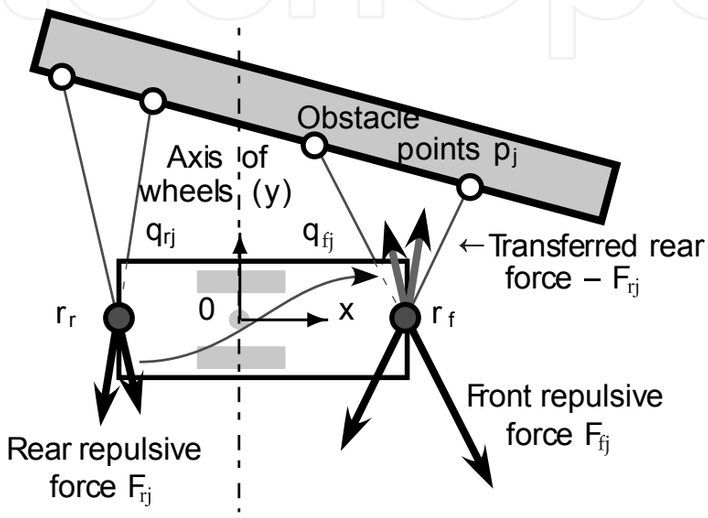

Fig. 8. Generation of repulsive forces from obstacle points.

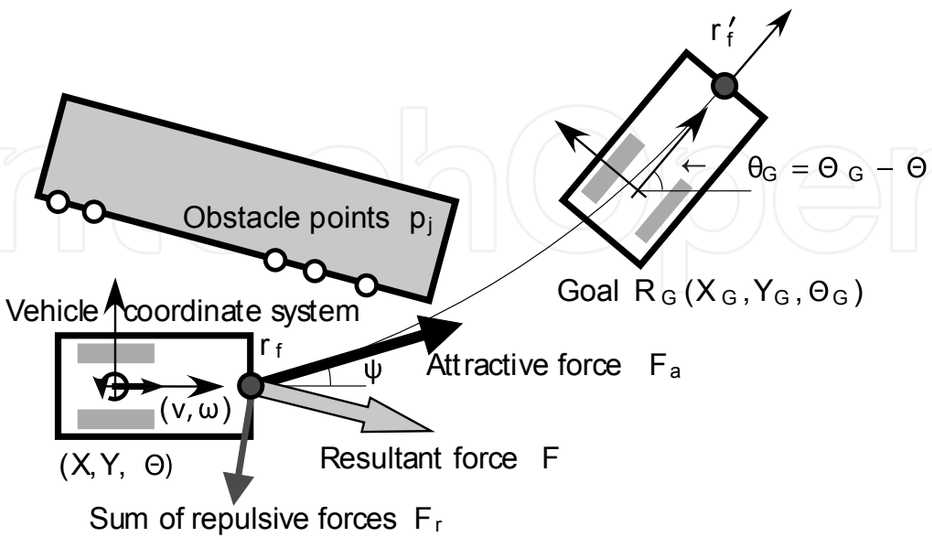

Fig. 9. Generation of attractive force and determination of velocity for avoidance.

Next, an attractive force $\boldsymbol{F_a}(|\boldsymbol{F_a}| = 1)$ pulls the front action point $\boldsymbol{r_f}$ of the vehicle toward the goal position as shown in Fig. 9. This attractive force is the tangential vector at the front action point $\boldsymbol{r_f}$ to the circle which comes in contact with the goal orientation of the front action point $\boldsymbol{r'_f}$. Without any obstacles, the vehicle moves on this circle and arrives at the goal position $\boldsymbol{R_G} = (X_G, Y_G, \Theta_G)^T$. The attractive force $\boldsymbol{F_a} = (\cos\psi, \sin\psi)^T$ is given by

$$\psi = 2\,\mathrm{atan2}\,(y'_G, x'_G) - \theta_G, \qquad \theta_G = \Theta_G - \Theta \tag{4}$$

$$\begin{bmatrix} x'_G \\ y'_G \end{bmatrix} = R(-\Theta) \begin{bmatrix} X_G - X \\ Y_G - Y \end{bmatrix} + R(\theta_G)\boldsymbol{r_f} - \boldsymbol{r_f} \tag{5}$$

where $R(\theta)$ is a rotation matrix by angle θ.

3.3 Resultant force and determination of vehicle's velocity

A resultant force $\boldsymbol{F}$ is obtained from the attractive and repulsive forces $\boldsymbol{F_a}$, $\boldsymbol{F_{fj}}$, $\boldsymbol{F_{rj}}$. Since the action points of their forces are not same, we can't simply add their force vectors. After the repulsive forces at the rear action point $\boldsymbol{F_{rj}}$ are transferred to the front action point by inverting their vectors $-\boldsymbol{F_{rj}}$, all force vectors are added at the front action point, because the front action point should be moved in the opposite direction of the rear repulsive force in order to move the rear body of the vehicle away from the rear obstacle point. That is, the front and rear action points have a relation like a "lever" of which the fulcrum is the midpoint of two wheels. Then, the resultant force at the front action point $\boldsymbol{F}$ is defined by

$$\boldsymbol{F} = \boldsymbol{F_a} + k_f \sum_{p_{jx}>0} \boldsymbol{F_{fj}} - k_r \sum_{p_{jx}<0} \boldsymbol{F_{rj}}, \qquad k_f + k_r = 1 \tag{6}$$

where the coefficients k_f, k_r represent the action rate of the front and rear repulsive forces. The determination of these coefficients are mentioned later.

Finally, the resultant force $\boldsymbol{F}$ pulls the front action point to move the vehicle. In other words, the translational and rotational velocities of the vehicle $(v, \omega)^T$ are determined in order that the front action point $\boldsymbol{r_f} = (x_f, 0)^T$ moves in the direction of the resultant force $\boldsymbol{F}/|\boldsymbol{F}| = (f_x, f_y)^T$.

$$\begin{bmatrix} v \\ \omega \end{bmatrix} = C \begin{bmatrix} f_x \\ \frac{f_y}{x_f} \end{bmatrix} \tag{7}$$

where C is the velocity coefficient. Since only the rate of translational and rotational velocities is obtained, suitable coefficient C should be given according to some limitations of velocity or acceleration. For example, when the maximum of the rotational velocity ω_{max} is specified, C becomes

$$C = \omega_{max} \frac{x_f}{f_y}, \qquad \text{if } |\omega| > \omega_{max} \tag{8}$$

3.4 Action rate of front and rear forces

How to determine the action rate of the front and rear repulsive forces k_f, k_r is discussed. When a vehicle avoids a block of obstacle as shown in Fig. 10, the force action rate doesn't affect vehicle's motion so much because repulsive forces mainly work at either action point. When a vehicle moves between walls on both sides, vehicle's motion isn't also sensitive to the action rate because repulsive forces at two points turn the vehicle in the same way. The case where the action rate affects vehicle's motion relatively is wall following. Repulsive forces are

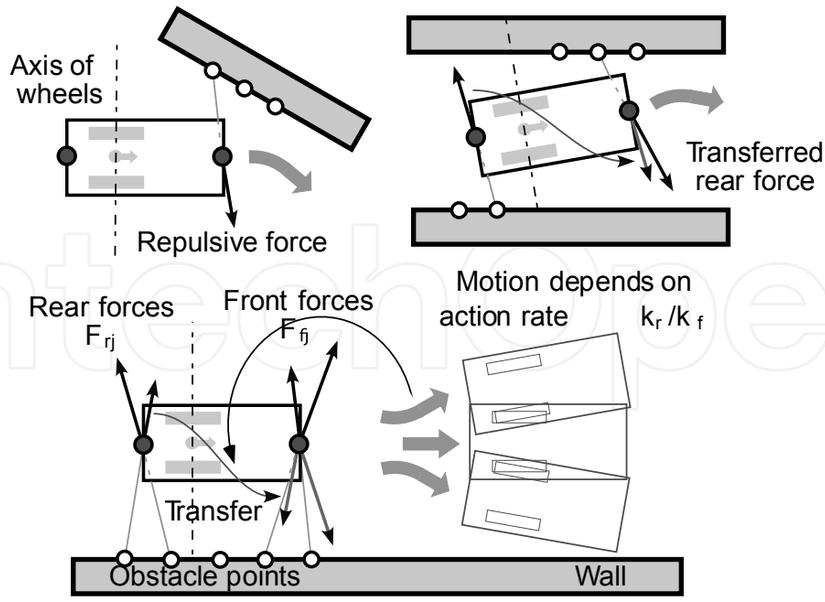

Fig. 10. Effect of action rate between front and rear forces on vehicle's motion. (Wall following is sensitive and others are not.)

generated at two action points to move their points away from the wall and their direction to turn the vehicle is different because they are treated like a lever of which the fulcrum is the midpoint of two wheels. During wall following, larger action rate of front forces k_f makes the vehicle turn away from the wall and larger action rate of rear forces k_r makes the vehicle turn close to the wall as shown in Fig. 10. Therefore, the force action rate should be determined so as that the vehicle goes straight along a wall, i.e. the resultant force vector $\boldsymbol{F}$ should be parallel to the wall without considering the attractive force $\boldsymbol{F_a}$. Let the components of repulsive force vectors at the front and rear action points in the vertical direction to the wall be F_{fyj}, F_{ryj} respectively, this condition becomes

$$k_f \sum F_{fyj} - k_r \sum F_{ryj} = 0 \tag{9}$$

Then, the action rate

$$\frac{k_r}{k_f} = \frac{\sum F_{fyj}}{\sum F_{ryj}} \tag{10}$$

is obtained. This depends on the shape of a vehicle, the detection area of a laser range sensor and so on.

The action rate for a rectangular vehicle is concretely calculated as shown in Fig. 11. Let the front length, rear length, width of a vehicle be a, b, $2c$, respectively. Let the distance between the wheels' axis and the laser range sensor be s_0 and the detection limit distance of the sensor be s. We can get the sum of components of repulsive force vectors in the vertical direction to the wall after repulsive forces, which are inversely proportional to the squares of the distances between the vehicle's body and the wall, are calculated. When the gap between a vehicle and a wall is d, they are given by

$$\sum F_{fyj} = \frac{KD^3}{d^2} I(a, -\phi_0, \phi_1) + KDI(a, \phi_1, \phi_3) \tag{11}$$

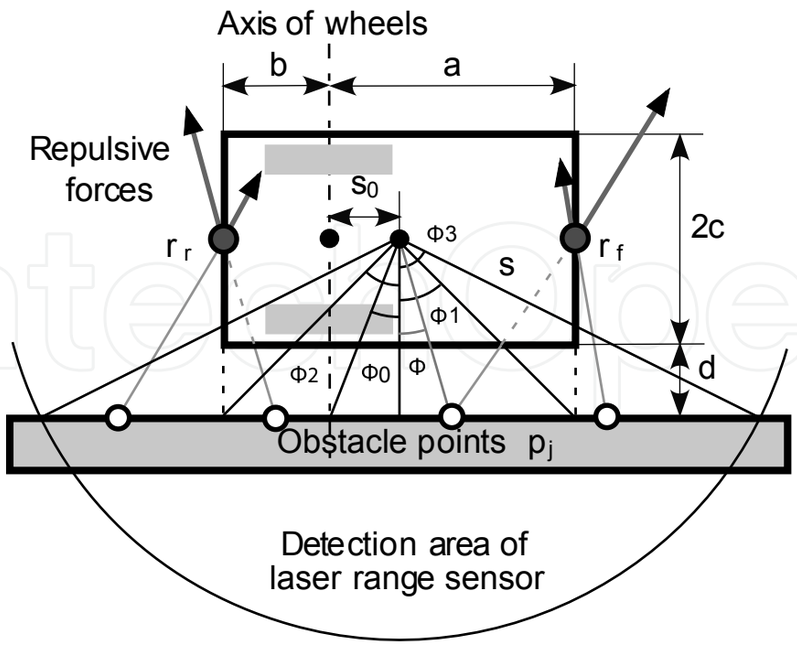

Fig. 11. Geometry of vehicle's body and repulsive forces during wall following.

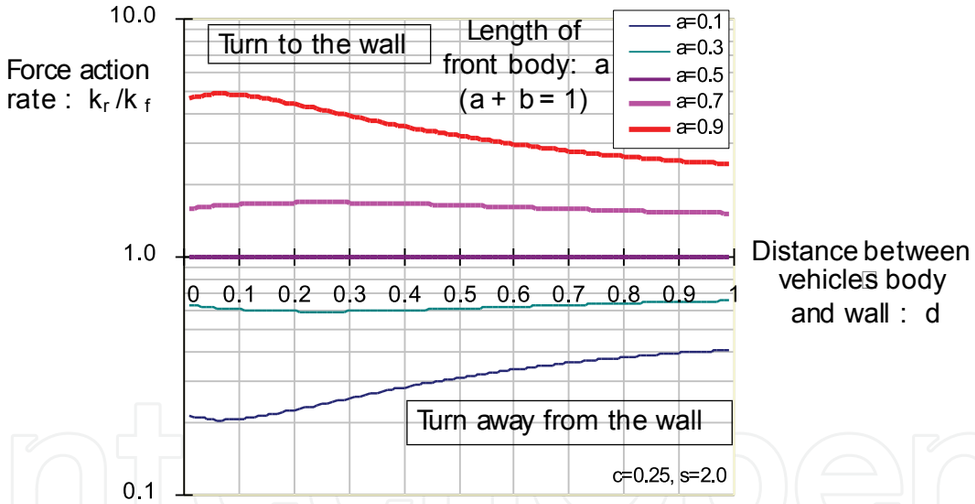

Fig. 12. Force action rate k_r/k_f to go straight along a wall.

$$\sum F_{ryj} = \frac{KD^3}{d^2} I(-b, -\phi_2, -\phi_0) + KDI(-b, -\phi_3, -\phi_2) \tag{12}$$

$$I(\alpha, \phi_s, \phi_e) = \int_{\phi_s}^{\phi_e} \frac{d\phi}{((\alpha - s_0 - D\tan\phi)^2 + D^2)^{\frac{3}{2}}}, \qquad D = c + d \tag{13}$$

where ϕ is the angle from the sensor to an obstacle point on the wall, ϕ_0, ϕ_1, ϕ_2, ϕ_3 are the angles from the sensor to the intersections between the wall and the wheels' axis, the front line of the body, the rear line of the body, the circle of detection limit of the sensor. Finally, the

action rate becomes

$$\frac{k_r}{k_f} = \frac{D^2 I(a, -\phi_0, \phi_1) + d^2 I(a, \phi_1, \phi_3)}{D^2 I(-b, -\phi_2, -\phi_0) + d^2 I(-b, -\phi_3, -\phi_2)} \tag{14}$$

This value is calculated by numerical integration.
Fig. 12 shows the relation between the distance from a wall d and the action rate k_r/k_f for a vehicle to go straight along the wall. In this calculation, it is assumed that the sensor is placed at the center of the vehicle ($s_0 = (a-b)/2$) and the length of the vehicle is normalized ($a + b = 1$). Some cases of the front and rear length of the vehicle with the width $2c = 0.5$ are shown in the graph. It can be seen that the action rate for the vehicle to go straight does not change so much according to the distance from the wall if the driven wheels are not close to either end of the body ($a = 0.3 \sim 0.7$). Even if the wheels are close to the end, there is no problem for obstacle avoidance because the action rate below these curves in the graph makes the vehicle turn away from the wall. When the front length a is short (Ex. $a = 0.1$), the minimum of the curve should be taken for the action rate. When a is long (Ex. $a = 0.9$), the value on the curve at a certain distance should be taken for the action rate because it makes the vehicle turn away from the wall if the vehicle goes inside its distance.

4. Simulation

Range of laser range sensor	$0 \sim 1$ [m]
Directional resolution of lager range sensor	1 [deg.]
Sampling time for control: Δt	0.1 [s]
Coefficient of repulsive force: K	0.004
Coefficient of velocity: C	0.2
Maximum angular velocity: ω_{max}	0.2 [rad/s]

Table 1. Standard parameters for simulation

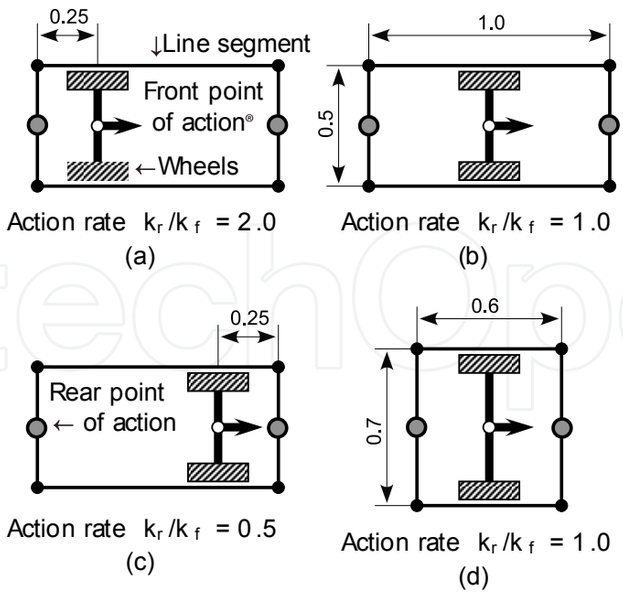

Fig. 13. Shape of vehicles for simulation

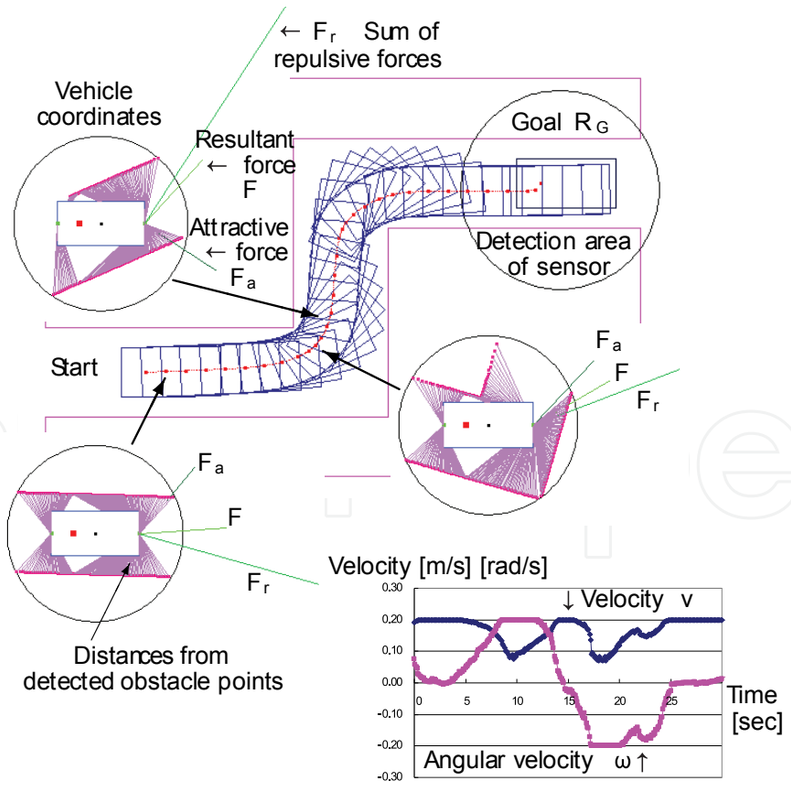

Fig. 14. Simulation result of the vehicle with shape (a).

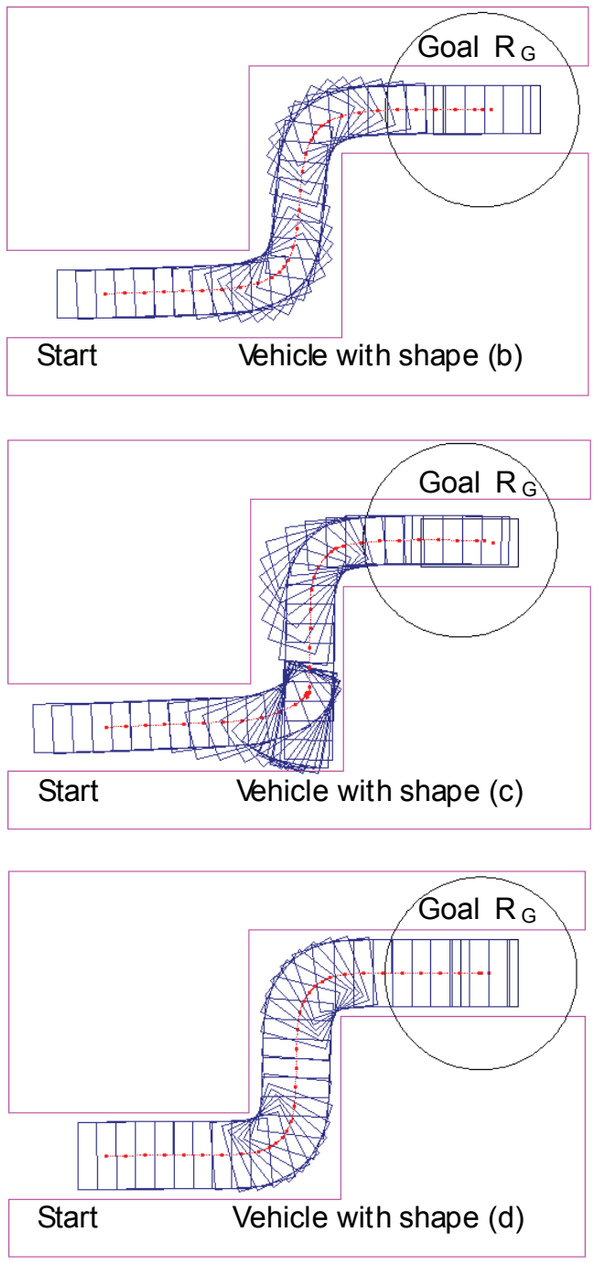

Fig. 15. Simulation results of vehicles with various shape.

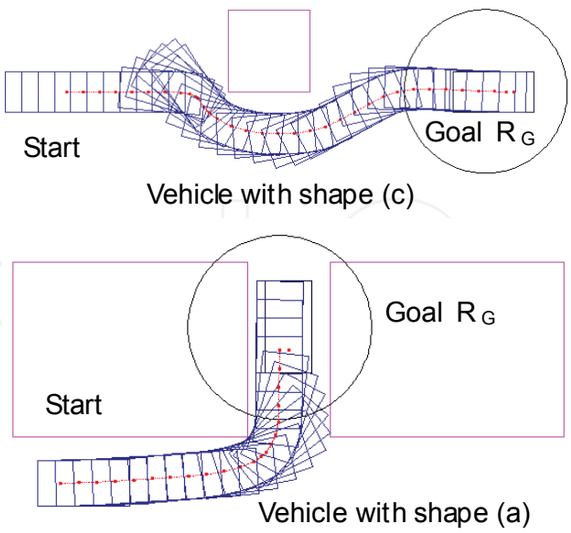

Fig. 16. Simulation results for various environment.

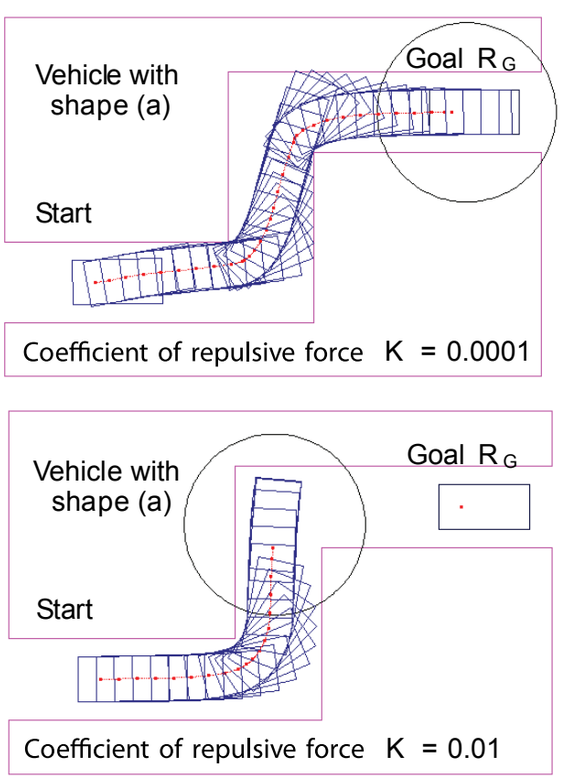

Fig. 17. Simulation results by using various coefficient of repulsive force.

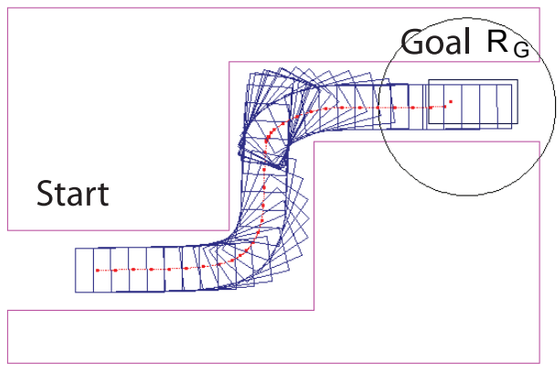

Fig. 18. Escape from local minimum by decreasing coefficient of repulsive force (When the vehicle stopped at Fig.17, coefficient of repulsive force K was temporarily decreased from 0.01 to 0.001 in 1 second.)

Our proposed method of local obstacle avoidance has been tested. All simulation programs were written in C language on PC Linux system. Table 1 shows standard parameters for the simulation. We assumed the following situation. A laser range sensor is mounted on the center of the rectangular body of a vehicle. Since the scan resolution angle is 1 degree, the max. number of detected obstacle points is 360. An obstacle point is calculated as the nearest intersection of obstacles and a direction of a laser range sensor within its detection area. Scan time is short enough to be neglected as compared with vehicle's speed. 4 types of vehicle's bodies were prepared as shown in Fig. 13. The action rate of the front and rear repulsive forces k_f, k_r was determined for each body by Equation (14).
Fig. 14 $\sim$ 17 are simulation results. Start and goal position were given as shown in each figure. Fig. 14 shows the generated path for the vehicle with shape (a) to pass through a narrow crank course. It can be seen that a smooth collision free path considering both rectangular body and motion constraint is generated by our proposed method. Obstacle points detected by the laser range sensor $\boldsymbol{p_j}$, distances between the vehicle's body and them, sum of repulsive forces $\boldsymbol{F_r}$, attractive forces $\boldsymbol{F_a}$ and resultant forces to avoid obstacles $\boldsymbol{F}$ are also shown in the vehicle coordinate system at some positions (See each circle in Fig. 14). A collision free direction can be determined from the sensor information directly. Moreover, the translational and rotational velocities of the vehicle v, ω are plotted in the graph and we can see that they changes smoothly.
Fig. 15 shows the cases of other vehicles' bodies and Fig. 16 shows the cases of other environments. It turns out that our proposed method is effective for various situations. Fig. 17 shows the results for various coefficient of repulsive force $K = 0.0001 \sim 0.01$. Larger coefficient generates the path farther away from obstacles, however, it isn't too sensitive (See also Fig. 14 of $K = 0.004$). When the coefficient is large, there seen some cases where the vehicle gets stuck at a local minimum. Many algorithms (Liu et al., 2000) to escape from the local minimum have been already proposed for general potential field method and some of them can be also applied to this case. For example, when a vehicle is stopped for a while like Fig. 17, it can escape from this local minimum by decreasing the coefficient of repulsive force K temporarily (Fig. 18).

5. Experiment

Navigation experiments were made by a powered wheelchair as shown in Fig. 19. This wheelchair has two powered wheels ("JW-I" manufactured by Yamaha Motor Co., Ltd., Wheel: 24[inch], Max. speed: 0.86[m/s]) with rotary encoders (2400[p/r]) and their velocities are controlled by PC (PI control every 0.05[sec]). Two laser range sensors ("URG-04LX" man-

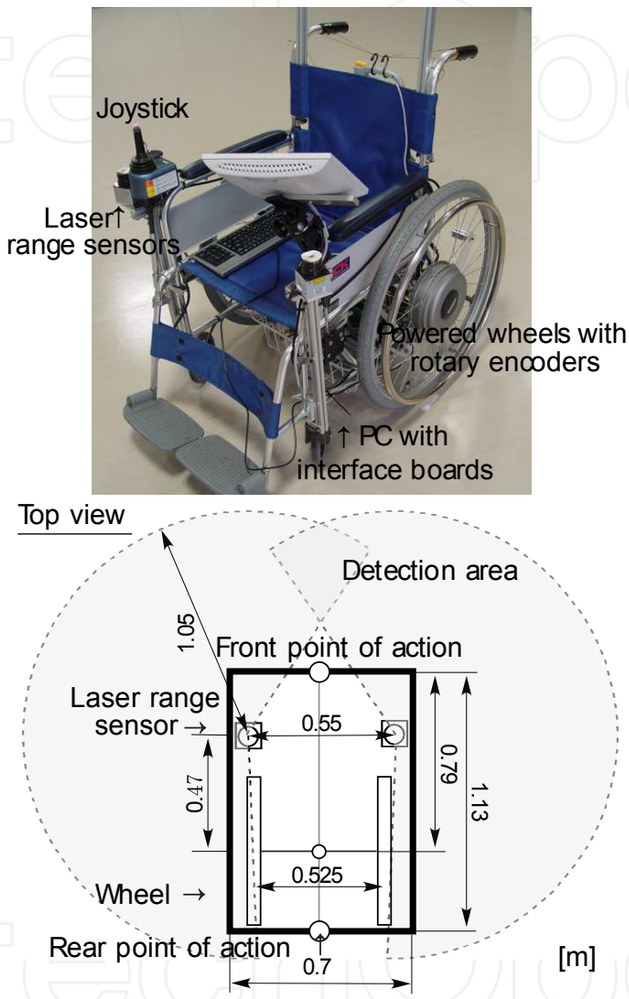

Fig. 19. Wheelchair setup and approximation to rectangular body to for experiment

ufactured by Hokuyo Automatic Co., Ltd., Range: 4[m], Resolution: ±10[mm], RS232C: 115.2[kbps]) are mounted at the both arm ends of the wheelchair not to disturb a user and not to be disturbed by a user. Their heights are 0.67[m] from the floor. After our proposed algorithm of obstacle avoidance was implemented to this wheelchair, navigation experiments were done in the environment as shown in Fig. 20. Table 2 shows parameters for the experiment. The shape of the wheelchair is approximated by a rectangle (Fig. 19), of which size is a little larger (1 ∼ 2cm) than the real body.

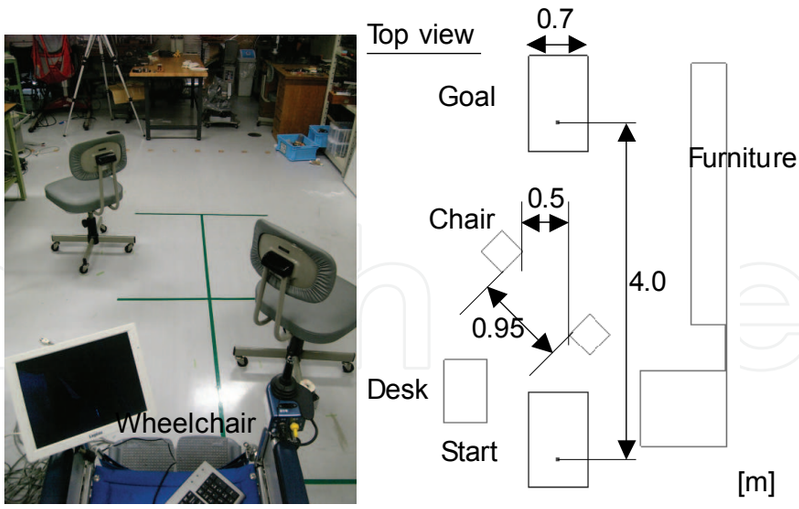

Fig. 20. Environment of navigation experiment

Range of laser range sensor	$0.2 \sim 1.05$ [m]
Directional resolution of lager range sensor	1.08 [deg.]
Sampling time for control: Δt	0.2 [s]
Coefficient of repulsive force: K	0.002
Coefficient of velocity: C	0.2
Maximum angular velocity: ω_{max}	0.2 [rad/s]
Action rate: k_r/k_f	0.6

Table 2. Parameters for navigation experiment

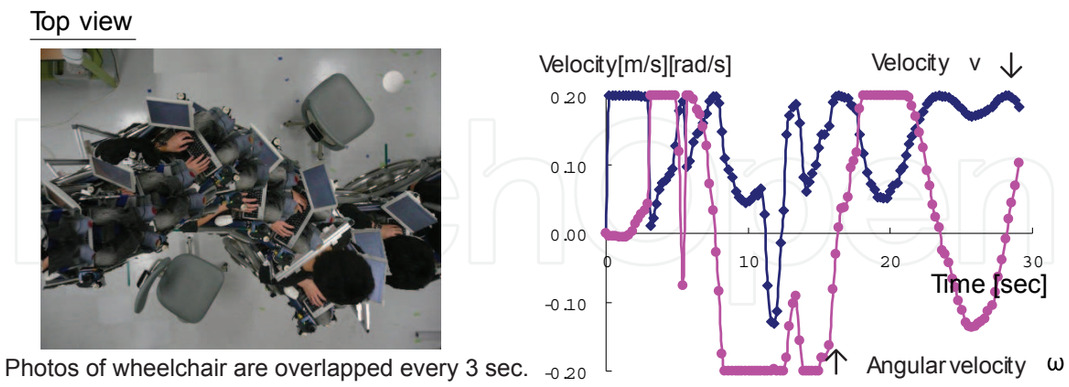

Fig. 21. Experimental results of trajectory and velocity

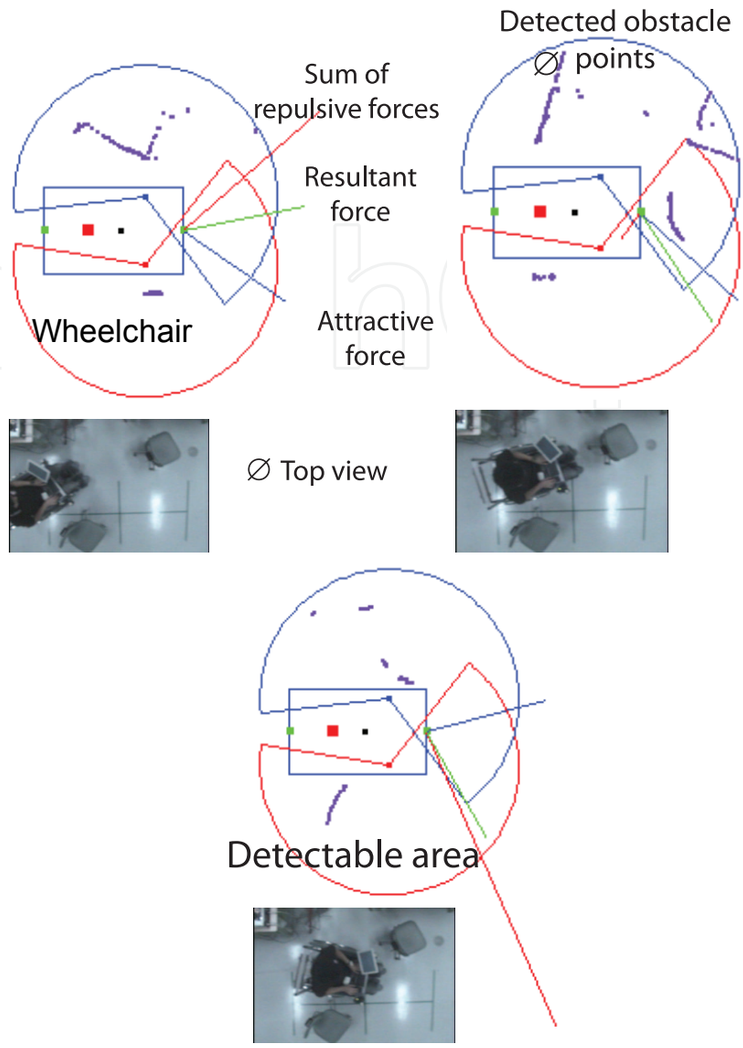

Fig. 22. Experimental results of sensor data at some places

Fig. 21 and Fig. 22 are experimental results. They shows the trajectory, velocity, and sensor data during the navigation. The autonomous wheelchair succeeded to avoid obstacles such as chairs, desks, and furniture and passed smoothly through the narrow space between chairs. The velocity data shows that the velocity was not always smooth in the experiment because the sensor sometimes failed to detect obstacle points. This failures can be seen in the sensor data at some places. One reason is that the sensor can't always catch the reflected laser light owing to the condition of obstacle surfaces. Another reason is that the shapes of obstacles changes according to the height of the sensor. It can be seen in Fig. 22 that the laser range sensor detected the back of a chair, not the seat of it, for example. 3D data of obstacles should be detected for practical use.

6. Application

An application of the obstacle avoidance function for an intelligent wheelchair is presented. It is an assist system of joystick operation to avoid obstacles for wheelchair users. In stead of giving a goal, the direction of the tilted joystick is assigned to the attractive force vector $\boldsymbol{F_a}$ in the proposed potential field method.

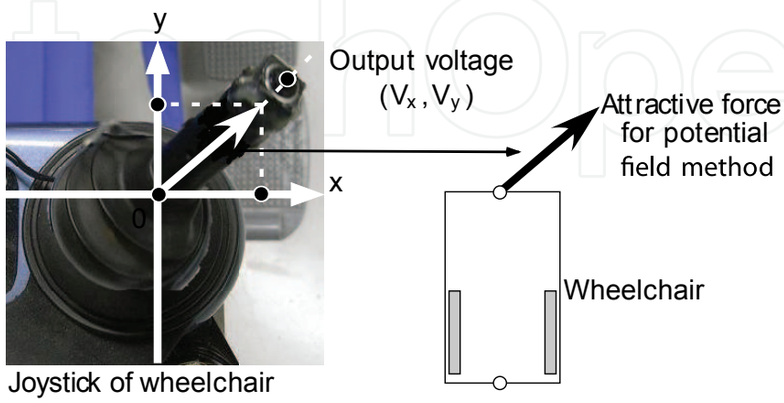

Fig. 23. Assist system of joystick operation to avoid obstacles

Let the 2D output voltages of the joystick device be $(V_x, V_y)^T$, the attractive force becomes

$$\boldsymbol{F_a} = \frac{\boldsymbol{V}}{|\boldsymbol{V}|}, \qquad \boldsymbol{V} = \left(\frac{V_x}{V_{xmax}}, \frac{V_y}{V_{ymax}} \right)^T \tag{15}$$

where $(V_{xmax}, V_{ymax})^T$ is the maximum of the output voltage. Then, the angle of the tilted joystick is assigned to the speed of the wheelchair $(v, \omega)^T$. Instead of Equation (7), the following equation is used.

$$\begin{bmatrix} v \\ \omega \end{bmatrix} = |\boldsymbol{V}| C \begin{bmatrix} f_x \\ \frac{f_y}{x_f} \end{bmatrix} \tag{16}$$

When there are no obstacles, the wheelchair moves as operated by the joystick. When wheelchair is going to collide with obstacles, the joystick operation is corrected by the potential field method. This system enables obstacle avoidance without precise operation of the wheelchair.

This assist system of joystick operation was tested in the same environment as the navigation experiment (Fig. 20). The user didn't operate the joystick precisely. Fig. 24 shows the trajectory of the wheelchair, the direction of the joystick, and the angle of the resultant force to move the wheelchair. It can be seen that the wheelchair succeeded to avoid chairs smoothly though the joystick operation by a user is rough. By this assistance of obstacle avoidance, a user can use the wheelchair easier with less joystick operation, even in the place where is difficult for he / her to pass through.

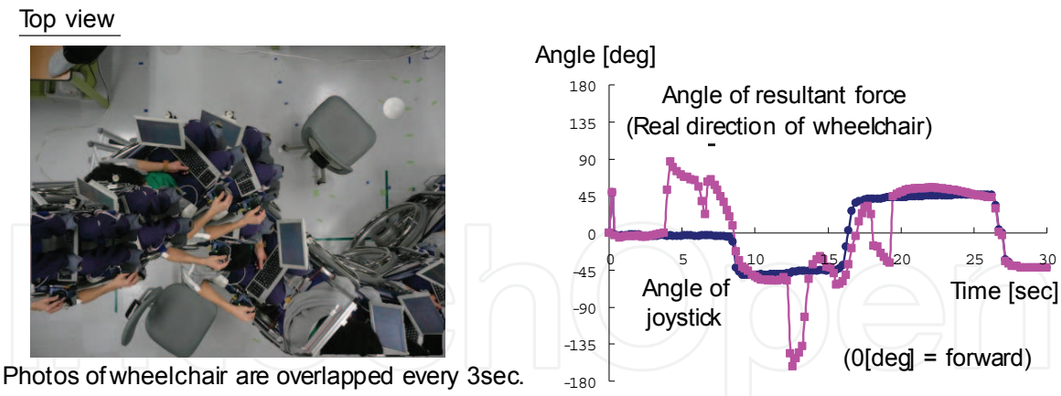

Fig. 24. Experimental results of assist system to avoid obstacles

7. Conclusion

In this chapter, a practical method of local obstacle avoidance for a nonholonomic vehicle with rectangular body has been proposed. Simple potential field directly using local sensor data is applied. Repulsive forces according to distances between obstacles and vehicle's body are generated at either front or rear point of action on the vehicle and their forces are treated like a lever. Both motion constraint and shape of a vehicle can be considered by this simple idea. Simulation results for various situations and experimental results by a wheelchair have proved effectiveness of our algorithm. Although this method has a disadvantage of local minima as well as general potential field method, it is intended for practical use because adequate path for local obstacle avoidance can be obtained with a little computing power. Furthermore, this algorithm may be applied to not only vehicles with two independently driven wheels but also car-like vehicles. Some improvements of the intelligent wheelchair such as 3D obstacle sensing and haptic joystick for obstacle avoidance, and consideration about general shape of vehicles are remained for our further works.

8. References

Kavraki, L. et al. (1996). Probabilistic Roadmaps for Path Planning in High Dimensional Configuration Spaces, *IEEE Transaction on Robotics and Automation*, Vol. 12, No. 4, pp. 566-580

Khatib, O. (1986). Real-Time Obstacle Avoidance for Manipulators and Mobile Robots, *International Journal of Robotics Research*, Vol. 5, No. 1, pp. 90-98

Kondak, K. & Hommel, G. (2001). Computation of Time Optimal Movements for Autonomous Parking of Non-Holonoimic Mobile Platforms, *Proceedings of 2001 IEEE International Conference on Robotics and Automation*, pp. 2698-2703.

Latombe, J. C. (1991). Robot Motion Planning, *Kluwer Academic Publishers*,

Laumond, J. P. et al. (1994). A Motion Planners for Nonholonomic Robots, *IEEE Transaction on Robots and Automation*, Vol. 10, No. 5, pp. 577-592

Liu, C. et al. (2000). Virtual Obstacle Concept for Local-minimum-recovery in Potential-field Based Navigation, *Proceedings of 2000 IEEE International Conference on Robotics and Automation*, pp. 983-988

Minguez, J. et al. (2006). Abstracting Vehicle Shape and Kinematic Constraints from Obstacle Avoidance Methods, *Autonomous Robots*, Vol. 20, pp. 43-59

Ramirez, G. & Zeghloul, S. (2001). Collision-free Path Planning for Nonholonomic Mobile Robots Using a New Obstacle Representation in The Velocity Space, *Robotica*, Vol. 19, pp. 543-555

Rimon, E. & Koditschek, D. E. (1992). Exact Robot Navigation Using Artificial Potential Functions, *IEEE Transaction on Robotics and Automation*, Vol. 8, No. 5, pp. 501-518.

Schwartz, J. T. & Sharir, M. (1983). On the Piano Movers' Problem: I. The Case of a Two-dimensional Rigid Polygonal Body Moving amidst Polygonal Barriers, *Communications on Pure and Applied Mathematics*n, Vol. 36, pp. 345-398.

Strobel, M. (1999). Navigation in Partially Unknown, Narrow, Cluttered Space, *Proceedings of 1999 IEEE International Conference on Robotics and Automation*, pp. 28-34

Ulrich, I. & Borenstein, J. (2000). VFH*: Local Obstacle Avoidance with Look-Ahead Verification, *Proceedings of 2000 IEEE International Conference on Robotics and Automation*, pp. 2505-2511

Factory Automation

Edited by Javier Silvestre-Blanes

ISBN 978-953-307-024-7
Hard cover, 602 pages
Publisher InTech
Published online 01, March, 2010
Published in print edition March, 2010

Factory automation has evolved significantly in the last few decades, and is today a complex, interdisciplinary, scientific area. In this book a selection of papers on topics related to factory automation is presented, covering a broad spectrum, so that the reader may become familiar with the various fields, and also study them in more depth where required. Within various chapters in this book, special attention is given to distributed applications and their use of networks, since it is one of the most relevant subjects in the evolution of factory automation. Different Medium Access Control and networks are analyzed, while Ethernet and Wireless networks are looked at in more detail, since they are among the hottest topics in recent research. Another important subject is everything concerning the increase in the complexity of factory automation, and the need for flexibility and interoperability. Finally the use of multi-agent systems, advanced control, formal methods, or the application in this field of RFID, are additional examples of the ideas and disciplines that experts around the world have analyzed in their work.

INTECH
open science | open minds

InTech Europe
University Campus STeP Ri
Slavka Krautzeka 83/A
51000 Rijeka, Croatia
Phone: +385 (51) 770 447
Fax: +385 (51) 686 166
www.intechopen.com

InTech China
Unit 405, Office Block, Hotel Equatorial Shanghai
No.65, Yan An Road (West), Shanghai, 200040, China
中国上海市延安西路65号上海国际贵都大饭店办公楼405单元
Phone: +86-21-62489820
Fax: +86-21-62489821

IntechOpen